Chemical Engineering Journal 427 (2022) 131856

Contents lists available at ScienceDirect

Chemical Engineering Journal

journal homepage: www.elsevier.com/locate/cej

Azo dye containing wastewater treatment in earthen membrane based unplanted two chambered constructed wetlands-microbial fuel cells: A new design for enhanced performance

Yamini Mittal [a,b], Sudatta Dash [a], Pratiksha Srivastava [c], Pravat Manjari Mishra [a], Tejraj M. Aminabhavi [d,e,*], Asheesh Kumar Yadav [a,*]

[a] CSIR-Institute of Minerals and Materials Technology, Bhubaneswar, Odisha 751013, India
[b] Academy of Scientific and Innovative Research (AcSIR), Ghaziabad, Uttar Pradesh 201002, India
[c] Australian Maritime College, College of Sciences and Engineering, University of Tasmania, Launceston 7248, Australia
[d] School of Advanced Sciences, KLE Technological University, Hubballi, Karnataka 580 031, India
[e] School of Engineering, Faculty of Science and Engineering, Macquarie University, Sydney, NSW 2109, Australia

ARTICLE INFO

Keywords:
Constructed wetland cum microbial fuel cell
Methyl orange
Chemical oxygen demand
Metagenomic analysis
Phytotoxicity

ABSTRACT

This investigation is the first of its kind to enhance detoxification of azo dye and other pollutants containing wastewater using an innovative earthen membrane-based two-chambered constructed wetland cum microbial fuel cell (CW-MFC). The present innovative design simulates the core of a shallow unplanted CW-MFC, which runs the sequential anaerobic and aerobic regimes without mixing of the cathodic and anodic wastewater. The obtained results revealed 94.04 ± 2.87% chemical oxygen demand (COD) and 94.22 ± 1.33% azo dye removal from the synthetic wastewater containing 550 mg/L initial COD and 50 mg/L Methyl orange (MO) azo dye, along with the current density and power density production of 544.6 mA/m^3 and 148.29 mW/m^3, respectively. The UV-visible spectrum demonstrated azo bond degradation in the anodic region, which was confirmed by the presence of sulphanilic acid as an intermediate of the azo dye degradation in the anodic effluent. The gas chromatography-mass spectrometry (GC-MS) analysis of anodic effluent proved the presence of an another intermediate, N.N-dimethyl-p-phenylenediamine (DMPD) and further confirms mineralization in the cathodic effluent with the elution of several mineralized polar compounds. Phytotoxicity study with *Vigna radiata, Triticum aestivum, and Cicer arietinum* indicated higher root growth rates (in comparison to control) of 30.72%, 13.53%, and 11.62% in the anodic effluent, whereas 69.70%, 60.28%, and 34.27% in the cathodic effluent, respectively, indicating decreased toxicity. The microbial analysis revealed a shift in microbial community of CW-MFC; the inoculum was abundant with *Methanomicrobia* class (18.55%), which shifted to class *Bacteroidetes* (13.99%) in the anodic region which was attributed to azo dye degrading bacteria. Whereas, cathodic microbial community consists of *Alpha* and *Gamma Proteobacteria* (59.50%), which are considered as the aromatic ring-degrading microbes.

1. Introduction

Azo dye is one of the major pollutants used in many industrial processes such as paper printing, food, cosmetics, and textile dyeing that are responsible for the release of a large quantity of azo dyes in wastewaters, thereby polluting the environment [1]. It is estimated that nearly one million tons of azo dyes are released each year from different industries into wastewater streams [2] of which about 20–30% come from the unstable dyes with an average concentration of 2000 mg/l [3]. These dyes when mixed with water bodies affect the photosynthesis process of the algae and other similar organisms in water bodies by preventing the light penetration, subsequently depleting oxygen, thereby adversely affecting the flora and fauna communities. Moreover, partial breakdown/degradation or treatment of azo dyes leads to the formation of mutagenic/carcinogenic intermediate compounds as these dyes constitute aromatic compounds with one or more —N═N— bonds (named azo

* Corresponding authors at: School of Advanced Sciences, KLE Technological University, Hubballi, Karnataka 580 031, India (T.M. Aminabhavi), Corresponding authors at: CSIR-Institute of Minerals and Materials Technology, Bhubaneswar, Odisha 751013, India (A.K.Yadav).
E-mail addresses: aminabhavit@gmail.com (T.M. Aminabhavi), asheesh.yadav@gmail.com (A.K. Yadav).

https://doi.org/10.1016/j.cej.2021.131856
Received 24 June 2021; Received in revised form 9 August 2021; Accepted 11 August 2021
Available online 21 August 2021
1385-8947/

bond) [4,5] The azo bond linkage is also responsible for the color due to its chromophoric functional group, making them highly stable owing to their complex aromatic rings and covalent azo bonds. Therefore, a complete destruction of these dyes has been a major challenge due to its recalcitrant nature.

In general, degradation/decolorization of azo bond occurs in two stages. The first stage involves reductive cleavage of azo bond, which generally takes place in an anaerobic environment, resulting in the formation of colorless, but potentially hazardous aromatic amines [6], which are resistant to further degradation in an anaerobic environment. Since microbial degradation of aromatic amines exclusively requires aerobic conditions, sequential anaerobic and aerobic conditions are proposed for a complete and adequate dye degradation [6,7].

Numerous physico-chemical processes [8] have been proposed for the destruction of azo dyes in wastewater treatment. Of these, coagulation/flocculation-based treatment methods require substantial quantity of chemicals, which can produce the sludge [8]. Adsorption and membrane filtration techniques can generate secondary sludge, which can pose further sludge handling and disposal issues [9]. Advanced oxidation processes (such as UV/H_2O_2, Fenton, ozonation, *etc.*) are quite effective, however these are energy and cost-intensive [4]. On the other hand, biological processes have been proven to be the cost-effective and eco-friendly alternatives to other treatment technologies [10]. Especially, Constructed wetlands (CWs) which is a conventional biological and passive treatment process suitable for the treatment of different types of industrial and municipal wastewaters. CWs have also been explored for several dye-containing wastewaters [11,12]. However, many challenges limit the adoption of CW, such as slow treatment rate and high land area requirement [13].

The recent progress in biological processes such as microbial fuel cells (MFCs) has been emerging as a sustainable treatment technology for azo dye-containing wastewaters even though up-scaling of MFC is still a major challenge. The other issues are low oxygen reduction rate (ORR) at low-cost cathode (such as carbon or graphite) leading to high overpotentials and low treatment kinetics in the MFC systems [13]. To overcome the individual challenges of CWs and MFCs, both the technologies have been proposed in a hybrid form of CW-MFC [14,15], where in case of CWs, the natural redox gradient occurs that can be suitable to build the MFCs [13,16]. Such a hybrid technology, *i.e.*, integration of constructed wetland with microbial fuel cell (CW-MFC) was first reported by Yadav et al., [17]. The CW-MFC contains anaerobic and aerobic regionswhich are embedded with electrodes (conductive material) as an electron acceptor and donor, which can assist to enhance the reaction processes in the anaerobic regions [18,19].

One of the first laboratory-scale CW-MFC was developed for methylene blue dye removal with > 75% dye removal even at higher dye loads of 2000 mg/L [14]. Later, a study by Fang et al., [20] achieved 91.24% decolorization from the active brilliant red X-3B (ABRX3) azo dye-containing wastewater along with 610 mV of voltage generation in CW-MFC, where increased decolorization was promoted by the electrodes [20]. Furthermore, methyl orange degradation in wastewater was studied in an open and closed-circuit CW-MFC to remove 75.59% and 87.60%, respectively [21,22]. A study with real dyestuff wastewater treatment in CW-MFC planted with *Fimbristylis dichotoma* achieved 82.2 ± 1.7% dye removal and 70 ± 2% Chemical oxygen demand (COD) reduction with a maximum power density generation of 198.8 mW/m^3 [23]. Furthermore, Acid orange 7 (AO7), Acid Red 18 (AR18), and Congo Red (CR) dye-containing wastewaters were treated in planted and non-planted CW-MFC that achieved decolorization as per the sequence: AR18 (96%) > AO7 (67%) > CR (60%) [24]. This study also concluded that decolorization efficiency was affected by the number of azo bonds and functional group positions. In all the above-mentioned studies, a typical single-chambered CW-MFC was employed to avoid the costly commercially available polymeric membranes, but the treatment efficiency and energy recovery were hampered; moreover, these studies still have severe issues of total azo dye mineralization/detoxification.

Thus, There is a need for an appropriate cost-effective CW-MFC technology with a high efficiency to achieve the total or very high dye mineralization and detoxification from wastewater. Interestingly, the earthen membrane was employed as the proton exchange membrane (PEM) in plant microbial fuel cells (PMFC) that achieved 99% of COD removal with current density generation of 242 ± 10.5 mA/m^3 [25]. The earthen membrane offered low internal resistance with a high power density compared to other membranes [26]. Thus, in the present study, an innovative earthen membrane-based two-chambered sequential anaerobic-aerobic CW-MFC was designed to achieve enhanced decolorization and detoxification of azo dye as well as their intermediate compounds from wastewater along with the electricity generation.

In this study, CW-MFC was separated into two chambers, *i.e.*, anaerobic (anodic) and aerobic chamber (cathodic) with a cost-effective porous earthen membrane acting as a PEM between the anode and the cathode of CW-MFC. It was hypothesized that azo bond cleavage and decolorization would take place in an anaerobic environment of the anodic chamber, while further toxic intermediate aromatic amine can be detoxified in the aerobic environment of the cathodic chamber. It was also hypothesized that this innovative design of the earthen membrane based two-chambered CW-MFC could resolve the issues that are generally emerging in a typical CW-MFC design. For instance, (i) it provides a novel CW-MFC design, which can lower the resistance value and hence, enhances the electricity generation and treatment performance; (ii) the new CW-MFC design will not allow the mixing of the catholyte with anolyte and (iii) the CW-MFC system will provide a sequential gravitational flow of wastewater for energy and cost-saving.

2. Materials and methods

2.1. Construction and working of the core of shallow unplanted CW-MFC

The outer cathodic or aerobic chamber of CW-MFC was constructed with a circular plastic container of 16.0-cm diameter and 16.0-cm height. At the centre of plastic container, an earthen pot was placed for creating an earthen membrane/layer, which can also work as an anodic chamber/anaerobic chamber. The earthen pot has an upper, middle, and lower diameter of 7.0 cm, 9.0 cm, and 7.0 cm, respectively, and a height of 12.0 cm. Both the chambers were filled with graphite granules (5.0–8.0 mm in diameter) to act as the conductive material-based anode and cathode electrodes. The cathodic and anodic chambers were embedded with a 112 mm × 13 mm (length × width) graphite rod as a charge collector/exchanger/dispenser.

The cathode charge dispenser was kept in contact with the atmospheric oxygen and placed 1.5 cm above the water level as per recently published study [27]. The anodic chamber and cathodic chamber have a void volume of 250 mL and 500 mL, respectively. An anodic sample was collected from the upper portion of the earthen pot for the analysis. The charge collectors of anodic and cathodic compartments were connected with an insulated copper wire of 1.0 mm for charge (electron) movement. An air sparger was provided at the bottom of the earthen pot in the cathodic chamber, which was connected to an aerator (Venus, AP-408A air pump, India). As a precautionary measure, the outer bottom portion of the earthen pot was covered with a high-density polyethylene liner (HDPE) for preventing air diffusion from the cathode chamber to the earthen pot, which was working as an anaerobic chamber as shown in Fig. 1. Both anodic and cathodic wires were connected with a resistance of 2000 Ω as a load.

2.2. Wastewater composition

Synthetic wastewater with glucose (550 mg/L) as an organic source was used throughout the study [24]. The synthetic wastewater constitutes: 0.111 g/L $NaHCO_3$, 0.0445 g/L KH_2PO_4, 0.0371 g/L $MgCl_2{\cdot}6H_2O$, 0.0301 g/L $CaCl_2{\cdot}2H_2O$, 0.1119 g/L $(NH_4)_2SO_4$, 0.0842 g/L $(NH_4)_2Fe(SO_4)_2{\cdot}6H_2O$. The trace metal mix composed of 2.86 g/L H_3BO_3, 1.81 g/

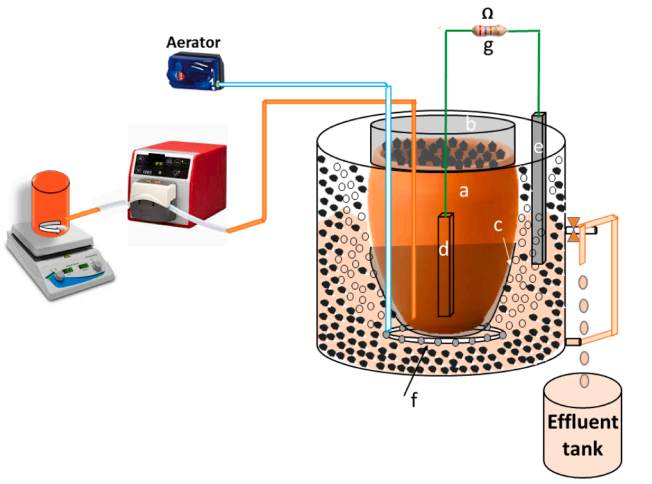

Fig. 1. Schematic diagram of the innovatively designed earthen membrane-based two chamber CW-MFC with sequential anaerobic and aerobic regimes. In this design, **a** earthen pot/layer acts as a proton exchange and oxygen/gas diffusion inhibiting membrane; **b** is an anode cover, which restricts the diffusion of air inside the anaerobic earthen chamber; **c** is HDPE liner covering the bottom part of the chamber for preventing oxygen/air diffusion inside the anaerobic chamber; **d** and **e** are the anode and cathode charge collectors/exchangers inserted in anode and cathode, respectively; **f** shows the aerator ring situated below the earthen pot and **g** is the resistance/load connected between anode and cathode.

L $MnCl_2{\cdot}4H_2O$, 0.222 g/L $ZnSO_4{\cdot}7H_2O$, 0.39 g/L $Na_2Mo_4{\cdot}2H_2O$, 0.079 g/L $CuSO_4{\cdot}5H_2O$ and 0.05 g/L $CoCl_2$. Tap water was used to prepare the synthetic wastewater with the afore-mentioned compounds and with a trace metal mix of 0.1 mL/L. The model azo dye used was Methyl orange (MO), purchased from HI Media Pvt. Ltd., India. During the experiment, initial concentration of 50 mg/L MO was mixed with synthetic wastewater with initial carbon concentration of 550 mg/L. The synthetic wastewater was thoroughly mixed through a magnetic stirrer (Tarsons, Model 4050, India) at 100–140 rpm speed to maintain the homogeneity of the influent. The entire experiment was carried out at 27 ± 2 °C.

2.3. Inoculation and experimental setup

The CW-MFC was inoculated with inoculum of the previously operated CW-MFCs in our laboratory. Initially, CW-MFC was acclimatized for nearly eight weeks with MO containing wastewater in a batch mode until stable voltage reading was recorded. After that, homogeneous wastewater containing MO dye was continuously fed into the bottom of the anode through a peristaltic pump (Watson Marlow 120S model, UK) at 24.66 mL/h. The aerator at the cathode was fixed to supply air at 2.4 L/min of flow rate and controlled by an automatic on-off timer (HPA digital timer, Australia) with repetitive 70 min followed by 10 min off cycles.

The CW-MFC was maintained to have a hydraulic retention time (HRT) of 27 h, wherein the wastewater retained in an anodic chamber for 9 h. The MO containing wastewater in the CW-MFC entered first to the lower anode chamber with the help of a peristaltic pump and then, the wastewater moved in the up-flow direction as it reached the upper portion of the anode chamber. As the wastewater reached the brim of the anode chamber, it oozed out in the outer cathode chamber by sliding through the walls of the anode chamber. Afterwards, it moved to the cathode chamber and gets discharged from the effluent pipe, which acted as an adjustable siphon tube, thus permitting half of the cathodic chamber to be filled and half empty. The half-empty upper cathodic chamber promoted more diffusion of oxygen, which further enhanced the electricity generation and wastewater treatment as shown in Fig. 1.

Unlike the single-chambered systems, in the current innovative design system, there was not mixing between the anolyte and catholyte as it was a double-chambered system that operated in conjunction with each other. Furthermore, the generated proton and electrons from the substrate metabolism in the anodic compartment were transferred to the cathode by the porous earthen pot membrane and through the electric wire, respectively.

2.4. Analysis, measurements, and calculations

Electricity generation was recorded in terms of the voltage on a daily basis with a digital handheld multi-meter (Fluke 17B, USA). Once the CW-MFC achieves steady state, the polarization curve was established by varying the external resistance from 90 MΩ to 1 Ω using a resistor box (Model 1040, time electronics, UK), and voltage was recorded every 15 min of interval. In order to obtain the polarization curve, a graph was plotted between voltage (V), power density (mW/m^3), and current density (mA/m^3) to acquire the ohmic, activation, and concentration losses. The current density and power density were calculated by dividing the anodic zone volume (m^3) of the CW-MFC. All the collected samples were filtered using a Whatman grade 1 filter paper (USA) before further analysis.

The MO concentrations in the anodic and cathodic samples were measured by a UV-Vis spectrophotometer (Agilent carry 100, USA). The standard curve of MO was plotted by fixing the wavelength at 464 nm and accordingly concentration of MO in samples were determined. The scanning of influent, anodic, and cathodic samples were performed on a UV-Vis spectrophotometer in the wavelength range between 200 and 800 nm to determine the intermediates from the azo dye decolorization and degradation, further % decolorization (DR) of the MO for the effluent of cathodic and anodic samples were calculated using Eq. (1):

$$\%\ DR = \frac{Influent{\cdot}dye\ concentration - Effluent\ dye\ concentration}{Influent{\cdot}dye\ concentration} \times 100 \quad (1)$$

The chemical oxygen demand (COD) was carried out in accordance with the closed reflux colorimetric method of APHA (American Public Health Association) [28] at 610 nm and % COD removal was calculated using Eq. (2):

$$\%\ COD\ removal = \frac{Influent\left(\frac{mg}{L}\right) - Effluent\left(\frac{mg}{L}\right)}{Influent\left(\frac{mg}{L}\right)} \times 100 \quad (2)$$

The dissolved oxygen (DO) and oxidation-reduction potential (ORP) of the upper and lower anodic region and cathodic regions were measured with DO and ORP probe attached to the HACH HQ-40D (USA), while the pH was measured using a pH meter (Eutech instruments cyberscan pH 1500, Canada).

The gas chromatography (GC) (QP2020 NX, Shimadzu, Japan) equipped with a DB-5 capillary column (30.0 m × 0.25 mm × 0.25 μm) coupled with mass spectrometry (MS) (QP2020 NX, Shimadzu, Japan) was used to validate the reduced azo dye intermediates. Prior to the GC-MS injection, 500 mL of the anodic and cathodic samples were collected, and their organic phases were extracted in chloroform using a separating funnel. The samples were dried using anhydrous Na_2SO_4 to remove the moisture or water content. Thereafter, the organic phases of both the samples were fully concentrated in a rotary evaporator (FL300, JULABO, Germany) and then collected in ethyl acetate solvent (HPLC grade).

For the GC-MS analysis, ultra-pure helium gas was used as a carrier and method was employed with 3 mL/min of purge flow at 250 °C of the injection temperature. The GC column was programmed and held at 40 °C for 1 min, then ramped at the rate of 10 °C/min to reach 250 °C for 15 min. The reduced MO intermediates were identified via GC-MS spectra as per the NIST (National institute of standards and technology) library [24].

2.5. Phyto-toxicity assessment with different seeds

Phyto-toxicity study was performed on the treated MO-containing wastewater to compare with without treated wastewater (influent) by identifying the root and shoot growth inhibition in the seedling of *Cicer arietinum, Triticum aestivum*, and *Vigna radiata*. To perform the toxicity experiments, petri-dishes were lined with three layers of paper cloth and seeds were sterilized before transferring to the petri dishes. Sterilization of the seeds was carried out to remove the dirt or any unwanted particles from the surface of the seeds. The seeds were sterilized by washing in 70.0% ethanol followed by further washing with 5.0% sodium hypochlorite by manual swirling, followed by six times of the distilled water wash and drying. Experiments performed in triplicates for all the three types of seeds with 20 seeds in each dish and 5 mL of the influent, anodic, and cathodic samples per petri-dish. Besides, the similar experiment was also performed on with tap water as a control experiment. Addition of respective 5 mL of wastewater samples or tap water was done each day in each petri-dish. The seeds were considered germinated when hypocotyl and radical appeared together. The root and shoot length measurement of the germinated seeds of *Cicer arietinum, Triticum aestivum*, and *Vigna radiata* were evaluated after six days. At the end of the exposure period, the % growth rate (GR) or % inhibition rate (IR) was calculated as per Eq. (3):

$$GR{\cdot}or{\cdot}IR\ (\%) = \frac{Root{\cdot}growth{\cdot}\text{in}{\cdot}tap{\cdot}water{\cdot}control\ (cm) - Root{\cdot}growth{\cdot}in{\cdot}influent{\cdot}or{\cdot}effluent{\cdot}sample(cm)}{Root{\cdot}growth{\cdot}\text{in}{\cdot}tap{\cdot}water{\cdot}control\ (cm)} \times 100 \quad (3)$$

If the obtained value from the above equation was positive, it was considered as inhibition (IR%) *i.e.*, the growth was lesser than the tap water/control, but if the obtained value was negative, it implied the growth (GR%) *i.e.*, growth was more than the tap water/control, where tap water was used as a reference.

2.6. Total metagenomic study of bacterial biofilms at anodic and cathodic regions

The microbial phylogenetic analysis (16S rRNA pyrosequencing) of anodic and cathodic regions as well as initial inoculum were performed. The biofilm formed at the graphite gravels of the anode and cathode regions was scraped with a sterile spatula and collected along with wastewater from those particular regions in a 250 mL sterilized sample bottle for the microbial analysis. The scrapped biofilm with wastewater was suspended in a 100 mM Tris-EDTA (TE) buffer to avoid the degradation of the sample. DNA was extracted from the Qiagen DNA easy Power Soil Kit (Qiagen, Germany) following the manufacturer's protocol. The V3-V4 region of 16S rRNA was amplified using the specific V3 Forward primer CCTACGGGNBGCASCAG and V4 Reverse primer GACTACNVGGGTATCTAATCC for diverse profiling.

For a better understanding of the approaches involved in the experimentation for azo dye degradation through the earthen membrane-based two chambered CW-MFC, a detailed flow chart is presented in Supplementary File, Fig S1.

3. Results and discussion

3.1. Environmental conditions of CW-MFC

The environmental conditions of different zones of CW-MFC were analyzed based on the values of DO, pH and ORP that are the major influential parameters in any biological treatment system. These parameters were examined throughout this study. At the lower region of the anode chamber, pH was found to be around 5.51 ± 0.39, while at the upper region, it was 5.94 ± 0.29. The pH at the upper anodic region was always somewhat less acidic compared to lower region, probably due to the supply of influent to the bottom of the anode chamber at first, which contained high organic and inorganic loads, thereby resulting in anaerobic conditions in the lower anodic region that could help to break down the co-substrate into fatty acids. However, production of fatty acids in the absence of oxygen can shift the pH to acidic condition; similar findings were also reported earlier [17]. The wastewater reaches to the upper anodic region, where it contains lesser organic and inorganic fractions due to their removal, thus resulting in a slight pH increase [29]. In the cathodic chamber, pH values were 6.16 ± 0.36 and 6.15 ± 0.45, respectively for lower and upper regions. The shift of cathodic pH to a less acidic value can be attributable to proton consumption in cathodic region; a similar observation was reported earlier by Srivastava et al., [30]. However, upon aeration, the expelled CO_2 from the solution by air stripping might also be one of the reasons for the increased pH values.

The DO profile of the influent, anode upper and lower regions, cathode upper and lower regions is shown in Fig. 2a. It can be seen that dissolved oxygen can be important in microbial activities of the CW-MFC systems. The DO in the initial wastewater was found to be 5.5–7 mg/L, while in the anode upper and anode lower regions, it was 1.71 ± 0.57 mg/L and 0.72 ± 0.27 mg/L, respectively. The low amount of DO in the anodic chamber could be due to high amount of oxygen-consuming organic and inorganic contents in the wastewater, which has resulted in an anaerobic environment. In addition, the attained DO range of 0.72–1.71 mg/L is suitable for functioning the electrochemically active bacteria (EABs) at the anode. Moreover, high amount of DO was reported as an inhibitor to EABs [31]. Similar DO conditions in anodic region of a vertical up-flow CW-MFCs have been also been reported [14]. In the cathode chamber, DO conditions at lower and upper regions were found to be 6.26 ± 1 mg/L and 6.72 ± 0.52 mg/L, respectively, resulting from an intermittent aeration. Furthermore, the presence of a lower level of DO in the anodic chamber suggest that the earthen membrane and HDPE liner acted as barriers for the diffusion of DO from cathodic chamber equipped with an aerator. Since DO is positively associated with ORP, ORP also significantly varied from −229.43 ± 43.02 mV to 84.03 ± 58.80 mV, indicating highly reducing and oxidative environment, while moving from anodic to cathodic chamber, respectively. Similar substantial alteration in ORP was also observed in other studies with the cathodic aeration in CW-MFC [32].

3.2. Chemical oxygen demand removal

The CW-MFC was evaluated for the COD removal and decolorization for 270 days. The COD removal efficiency in anodic and cathodic chambers is shown in Fig. 2b. The initial COD concentration of wastewater was 630 ± 29.48 mg/L, but the COD removal in anodic chamber was 60–70% for the initial six weeks, which corresponds to the remaining value of the COD to 250 ± 20.6 mg/L in the anodic effluent, however after six weeks, the COD removal was increased to 85%. The gradual increase in COD removal could be related to the development of incremental biofilm as the anaerobic heterotrophic microbes could use carbon as a source of energy as well as for their growth and metabolic

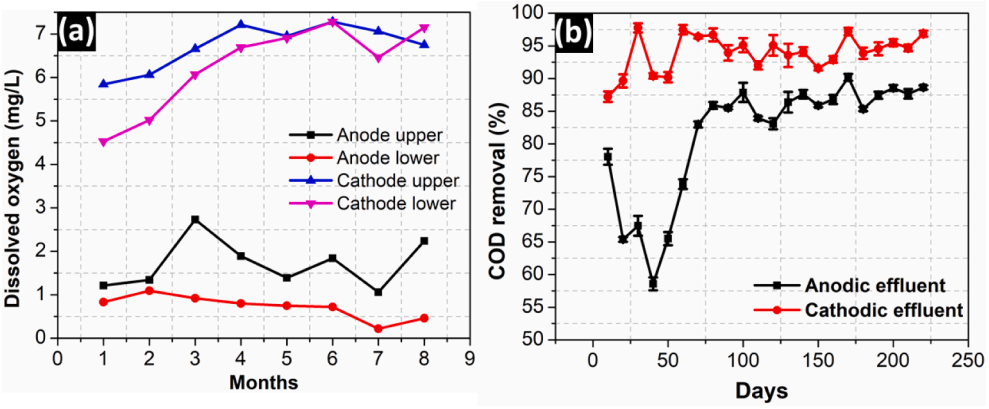

Fig. 2. (a) Cathodic and anodic dissolved oxygen profile of CW-MFC; and (b) percentage COD removal in anodic and cathodic effluent of CW-MFC.

activity [18]. It is also evident from the results that most of the COD removal occurred in an anaerobic chamber. The higher COD removal in CW-MFC may be the result of electron transfer from anode portion to cathode portion, resulting in higher oxidation of pollutants [16]. Hence, continuous electron transfer from anode to cathode would have accelerated the metabolic activity of the anaerobic bacteria along with the fast oxidation of the substrate. A similar mechanism was also proposed by other authors [33,34]. In the present study, we hypothesized that electrons were utilized in the azo bond reduction of MO, which would also have accelerated the COD removal in the anode. Moreover, the remaining 87 ± 17.24 mg/L was removed in the cathodic chamber, where COD decreased to 60 mg/L in the early days of the operation and later to 20 mg/L. In the cathode, sufficient oxygen supply could have also increased the biomass with time, resulting in an efficient removal of COD. In addition, the intermittently supplied oxygen might have promoted the aerobic oxidation that has led to the removal of remaining COD. The above results are in good agreement with published research [22], where the anode layer of CW-MFC closed-circuit contributed highest in COD removal.

3.3. Methyl orange decolorization and degradation

The decolorization of MO at different portions of CW-MFC was determined and shown in Fig. 3a. It was observed that 92.12 ± 2.62% decolorization took place in the anodic region, whereas some of MO was treated in the cathodic region.MO concentration in the effluent was 2.42 ± 1.33 mg/L. The majority of dye decolorization occurred in the anodic region due to suitable environmental conditions such as availability of the substrate, biomass and favourable redox potential. Redox potential of < -50 mV is imperative for the breakage of azo bond, which totally corroborates with the reductive environmental conditions (*i.e.,* −229.43 ± 43.02 mV) in the anode chamber of CW-MFC [22]. These results are in agreement with the published literature [22,24]. Moreover, surface adsorption onto the graphite and biomass could also attributedin dye removal. However, due to the saturation of graphite gravels and biomass, adsorption-like mechanisms could not be sustained for longer extended period [14].

In order to investigate the possible pathway of dye degradation, samples were collected from the influent, upper anodic region effluent, and cathode effluents,were analyzed via UV-visible spectra (Fig. 3a). The UV-Vis spectra of influent, anodic, and cathode effluent samples confirmed the azo bond cleavage as well as the degradation of MO. In case of influent wastewater, a strong absorbance band observed at 464 nm suggests denotation of the conjugated structure by the azo bond under the influence of electron-donating dimethyl amino group [35]. Another band at 270 nm may be related to π to π* transition in the aromatic rings. In anodic sample, no bands were observed at 464 nm and 270 nm, whereas a new band appeared at 248 nm, signifying that azo bond (—N═N—) cleavage has led to the formation of sulphanilic acid as confirmed by UV-Vis spectra of the standard sulphanilic acid solution shown in Fig. 3b; similar observations were also suggested by other researchers [35–37]. The degradation of dye in anodic effluent can be explained on the basis of the presence of electronegative sulphonyl group on the para position in MO, which can extract the electrons from —N═N— bond via resonance to convert it into an electrophilic and reduced form [38]. Hence, bio-electrochemical pathway behind the reduction of azo bond could be consumption of electrons generated with the oxidation of biodegradable substrate catalyzed by the anodic biofilm. It may be realized that these generated electrons are donated outside their cell wall by the electroactive microorganisms known as EABs or exoelectrogens [13], as depicted in Fig. 4.

As the anodic effluent reached the aerobic cathode chamber of the CW-MFC, the band observed in anodic effluent at 248 nm was significantly decreased, and the observed band was ten-times lower in absorbance than the anodic samples *i.e.*, from ≈ 3.35 to 0.36 (Fig. 3c). Such a significant decrease in absorbance from the anodic to cathodic regions is an indication of the decrease or disappearance of the aromatic rings of the effluent [7]. However, a sharp increase of sulphalinic acid in the anodic region depicts the accumulation of sulphanilic acid, while decline of the same band in cathodic region signifies its further degradation [6,36]. These results are in agreement with the general consensus that sulphalinic acid can only be degraded in an aerobic environment [39]. Moreover, further confirmation of MO mineralization from anodic and cathodic samples was carried out via GC-MS.

The UV-Vis spectra confirmed the formation of sulphalinic acid from the anodic samples. The GC-MS analysis indicates the formation of N, N-dimethyl-p-phenylenediamine (DMPD) intermediate from the anodic sample [40] and DMPD was eluted at a retention time of approximately 17.29 min with *m/z* of 136 as shown in Fig. 3d. Since the boiling point of sulphalinic acid is higher than the temperature limit of the gas chromatography, it was not detected in the GC-MS analysis. Moreover, from the MS fragmentations pattern, *m/z* peaks of the characteristic fragment ions were observed at 136, 108, 93, 88, 77, 60, and 18, which are in accordance with the reported results [36,40–42]. Since the anodic effluent flows down towards cathodic region, the total mineralization of MO occurred in the cathodic region, which was confirmed by GC-MS analysis (Fig. 3e). Since the aeration at the cathode provided sufficient electron acceptor for the degradation of azo dye intermediates, the degradation occurred more in the cathodic region. Thus, creating suitable ORP conditions for DMPD degradation, requires ORP of 120 mV [22], which is coherant with our achieved value of 140.2 mV in the cathodic chamber. In the effluent samples, no aromatic ring compound was detected (Fig. 3e). The compounds detected in the effluent samples were in the mineralized forms such as diethylpyrocarbonate, 1-Ethoxy-3-methyl-2-butene, 1,2-ethanediol/ monoacetate, 2,3-dimethylheptane, 2-pentanone,4-hydroxy-4-methyl, 1-butylnonyl acetate, which were

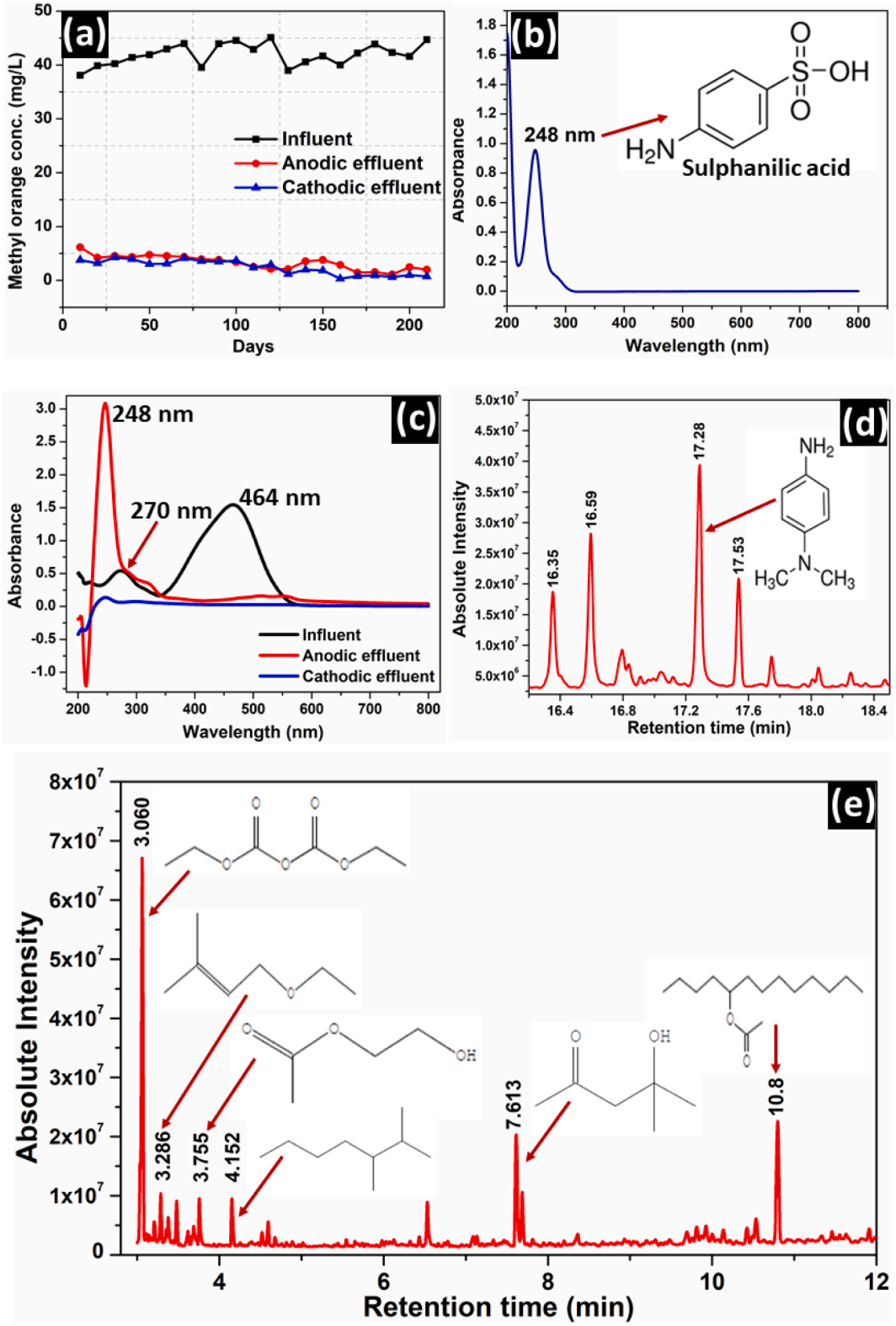

Fig. 3. **(a)** MO concentration in influent, anodic and cathodic regions of CW-MFC, **(b)** UV-Vis spectra of sulphanilic acid, **(c)** UV-Vis spectra of influent, anodic, and cathodic effluent **(d)** GC-MS chromatogram of the anodic effluent, and **(e)** GC-MS chromatogram of the cathodic effluent.

eluted at 3.060, 3.287, 3.753, 4.153, 7.613, 10.797, respectively [43,44]. Mineralization in the aerobic region can be due to the incorporation of oxygen atoms from O_2 into the aromatic rings of the intermediates before the fusion of ring, catalyzed by the oxido-reductase enzyme of both mono and di-oxygenases [7] as depicted in Fig. 4. Additionally, the results are in accordance with published work [39], where oxygen consumption was directly proportional to sulphanilic acid degradation. As per literature findings [45], when the anaerobic metabolites of azo dye were metabolized aerobically, the formation of smaller aromatic and polar compounds have led to the shift in the

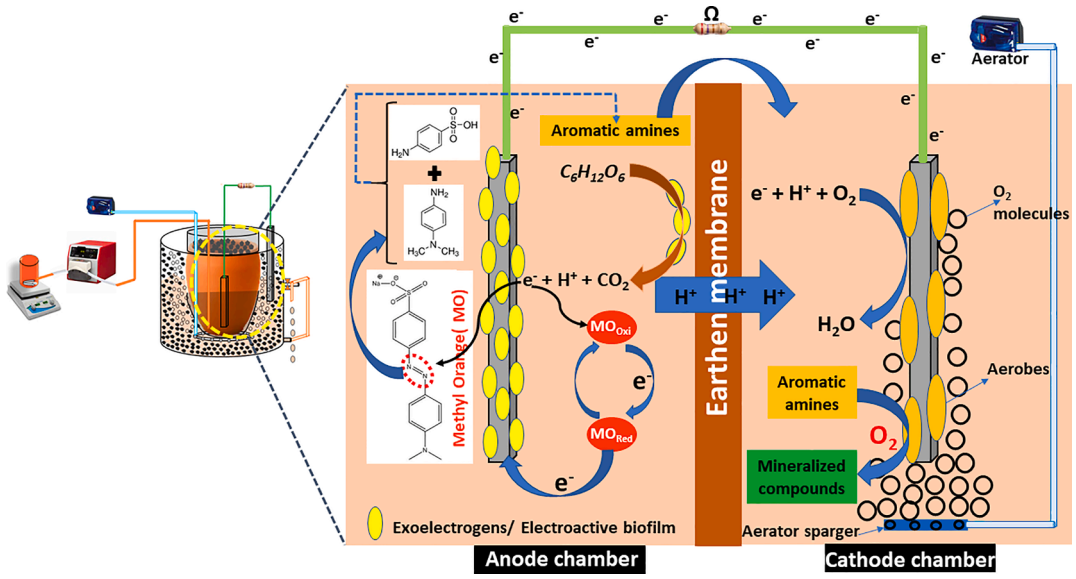

Fig. 4. Probable bio-electrochemical pathway for MO degradation/mineralisation. (For interpretation of the references to color in this figure legend, the reader is referred to the web version of this article.)

Table 1
Displays recent CW-MFC studies on simultaneous azo dye removal and electricity generation.

CW-MFC design	Dye	Initial COD concentration (mg/L);% COD removal	Initial dye concentration (mg/L)	Decolourisation efficiency (%)	HRT (in days)	Max. power density	Ref.
Batch single chambered	Methylene Blue (MB)	1500; 75	500	93.15	4	15.7 mW/m^2	[14]
Single chambered continuous vertical upflow	Reactive brilliant red X-3B (ABRX3)	180; 85.65	150	91.24	3	302 mW/m^3	[20]
Single chambered continuous vertical upflow	Reactive brilliant red X-3B (ABRX3)	300; 72.5	500	94.9	3	852 mW/m^3	[21]
Single chambered continuous vertical upflow	Methyl Orange (MO)	50; 56.20	450	87.6	3	81 mW/m^3	[22]
Single chambered continuous vertical upflow	Reactive brilliant red X-3B (ABRX3)	300; 60.76	300	92.7	3	117 mW/m^3	[46]
Single chambered continuous vertical upflow	Acid Red 18 (AR18)		500	91	1	8.67 mW/m^2	[47]
Single chambered continuous vertical flow	Real dyestuff wastewater	1580 ± 200 ;70 ± 2%	1712 ± 38 (*ADMI)	82.2 ± 1.7	3	198.8 mW/m^2	[23]
Single chambered continuous vertical flow	Acid Red 18 (AR18), Acid Orange 7 (AO7), Congo Red (CR)	AR18: 560; 74, AO7: 624	AR18: 200, AO7: 200, CR: 200	AR18: 96, AO7: 67, CR: 60	1	AR18: 1.58 mW/m^2, AO7: 1.13 mW/m^2, CR: 1.02 mW/m^2	[24]
Two-step horizontal sub-surface flow in batch	Real dyestuff wastewater	1058 ± 120; 74.10 ± 1.75	30170 ± 300 (*ADMI)	97.32 ± 1.90	4	197.94 mW/m^2	[48]
Earthen membrane-based two chambered CW-MFC	**Methyl Orange (MO)**	**550; 94.04 ± 2.87**	**50**	**94.22 ± 1.33**	**1.13**	**148.29 mW/m^3**	**Present study**

*ADMI- American dyes manufacturers institutes (denotes index value of mixed dye solution).

retention peak to lower value. Similar results can be visualized in the present study via the GC-MS data as shown in Fig. 3d and 3e.

Decolourisation efficiency and COD removal of data collected from different published sources along with the results obtained in present study using CW-MFC for the removal of azo dyes are compared in Table 1, wherein colour removal efficiency and COD removal data varied from 60.0% to 90.72% and 56.20% to 95%, respectively. The COD removal and decolourisation in the current work are comparable to those published in the literature [24], where the acid red 18 (initial concentration of 200 mg/L) and organics (initial concentration of 560 mg/L) showed 96% and 74% removal, respectively.

3.4. Electricity generation

The maximum current density and power density achieved were 544.6 mA/m^3 and 148.29 mW/m^3, respectively and the CW-MFC was characterized electrochemically by plotting the polarization curve as shown in Fig. 5a. The polarization study was conducted after achieving steady-state and in the initial phase of the experiment, accordingly external resistance of 2KΩ was decided based on the polarization study .

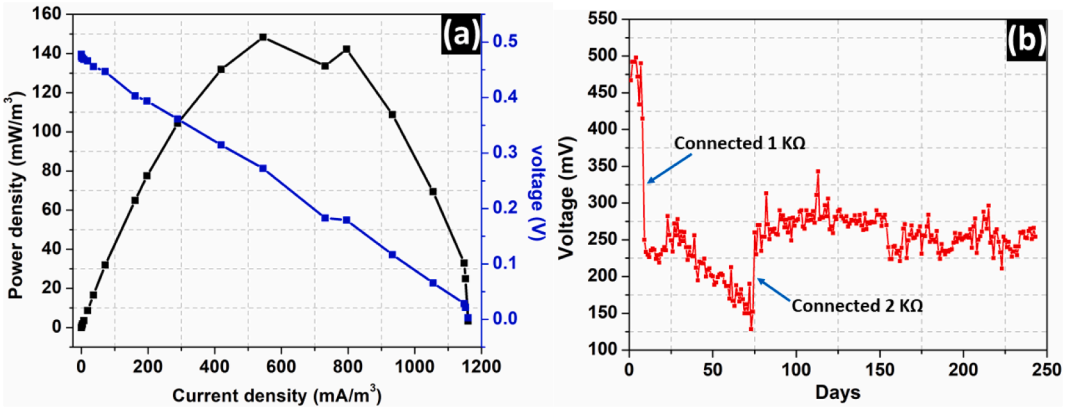

Fig. 5. **(a)** polarization curve of CW-MFC at varying resistances and **(b)** voltage profile of the earthen CW-MFC for the entire study.

The polarization curve provides a basic idea about the losses, which mainly affected the system performance such as less voltage output than the predicted thermodynamic ideal voltage. The observed losses were ohmic, activation and mass transfer [30,49]. These losses are recorded during the electrochemical reaction, mass transfer, and charge transfer in anodic and cathodic regions of the CW-MFC [16]. Anode and cathode electrodes were placed closer to each other to reduce cathodic ohmic losses, and hence protons have a small distance to travel [50]. It is also reflected with the CW-MFC design in the present study where protons had to travel through the porous earthen membrane up to a few mm. Also, the presence of intermittent aeration in cathodic region might have reduced the activation and mass transfer losses by fulfilling the oxidant (O_2) requirement, thereby promoting the power output of CW-MFC [30,32]. The negative value of -229.43 ± 43.02 mV ORP in anode and positive ORP of 84.03 ± 58.80 mV at the cathode created a high redox potential/potential difference between the anode and cathode, which further elevated the current flow and thereby, the electricity generation.

The three losses such as activation loss, ohmic loss, and concentration loss were observed in the polarization curve shown in Fig. 5a. The activation losses are depicted by the sharp decrease in the voltage, whereas ohmic loss was expressed by the slow declining nature of the voltage (almost in a linear manner). Moreover, concentration losses are symbolized by the rapid fall of voltage at the high current density [29]. Furthermore, voltage profile of CW-MFCis shown in Fig. 5b, where the highest voltage was achieved in CW-MFC at 498 mV in 2 KΩ resistance load. The higher voltage output can be due to the presence of MO, which could function as redox shuttle by reversibly oxidizing and reducing itself in the process of transferring electron to anode/solid electron acceptor thus accelerating the extracellular electron transfer [14], as depicted in Fig. 4. Additionally, in the voltage profile, there was an increase in the voltage, which further gradually decreased.

3.5. Phytotoxicity assessment

Phytotoxicity results of *Cicer arietinum*, *Triticum aestivum*, and *Vigna radiata* seeds revealed that dye-containing influent wastewater inhibited the germination and growth when compared to tap water control, wherein, the root growth inhibition of 51.10%, 68.83%, and 15.13% was observed for *C. arietinum*, *T. aestivum*, and *V. radiata*, respectively. On the contrary, increased seed germination and growth (in both root and shoot length) were observed in the anodic and cathodic effluents as shown in Table 2. Comparing the anodic effluent to cathodic effluent, root germination increased from 11.62% to 34.27% in *C. arietinum*; 13.53% to 60.28% in *T. aestivum*; and 30.72% to 69.70% for *V. radiata* seedlings. This signifies the decrease of toxicity level in cathodic effluent compared to anodic effluent as the seed germination and growth was higher in cathodic effluent samples than the upper anodic samples. This was attributed to the enhanced degree of mineralization in the subsequent aerobic treatment of the aromatic toxic by-products produced during the anerobic treatment in the anodic chamber. The present data indicate that sulphonated dyes were toxic for *C. arietinum*, *T. aestivum*; and *V. radiata* seedlings owing to the toxicity of both parental dye and their metabolized aromatic compounds. Moreover, the accumulation of dye in seedling tissues would cause the DNA impairment in plants cell, thereby hindering the growth [51]. Further, increased shoot germination and growth was also observed in case of all the grown seedlings compared to the tap water control. Similar results were also presented from other studies [52], where 13.33% increase in growth from the treated to the untreated dye wastewater was observed in the case of *V. radiata*. Moreover, the highest increase in germination and growth was noticed in *V. radiata* seedling due to its early seedling growth compared to other seeds. The increased growth in the anode upper and cathode effluents clearly indicate a reduction of aromatic MO metabolites to the mineralized compounds, which has reduced the phytotoxicity

Table 2
Phytotoxicity assessment with different seeds in the influent, anodic effluent, cathodic effluent, and tap water (chosen as control).

Vigna radiata	% Shoot inhibition rate (IR)/% growth rate (GR)	72.81 (IR)	1.62 (GR)	14.37 (GR)	-
	% Root inhibition rate (IR)/% growth rate (GR)	15.13 (IR)	30.72 (GR)	69.7 (GR)	-
	Mean shoot growth (in cm)	2.175	8.13	9.15	8
	Mean root growth (in cm)	1.29	1.987	2.575	1.52
Triticum aestivum	% Shoot inhibition rate (IR)/% growth rate (GR)	51.24 (IR)	10.24 (GR)	11.43 (GR)	–
	% Root inhibition rate (IR)/% growth rate (GR)	68.83 (IR)	13.53 (GR)	60.28 (GR)	–
	Mean shoot growth (in cm)	2.35	5.314	5.371	4.82
	Mean root growth (in cm)	1.2	4.371	6.171	3.85
Cicer arietinum	% Shoot inhibition rate (IR)/% growth (GR)	68.47 (IR)	23.1 (GR)	39.86 (GR)	–
	% Root inhibition rate (IR)/% growth rate (GR)	51.10 (IR)	11.62 (GR)	34.27 (GR)	–
	Mean shoot growth (in cm)	0.4571	1.785	2.028	1.45
	Mean root growth (in cm)	2.528	5.771	6.942	5.17
	Test solution	Influent	Anode effluent	Cathodic effluent	Tap water

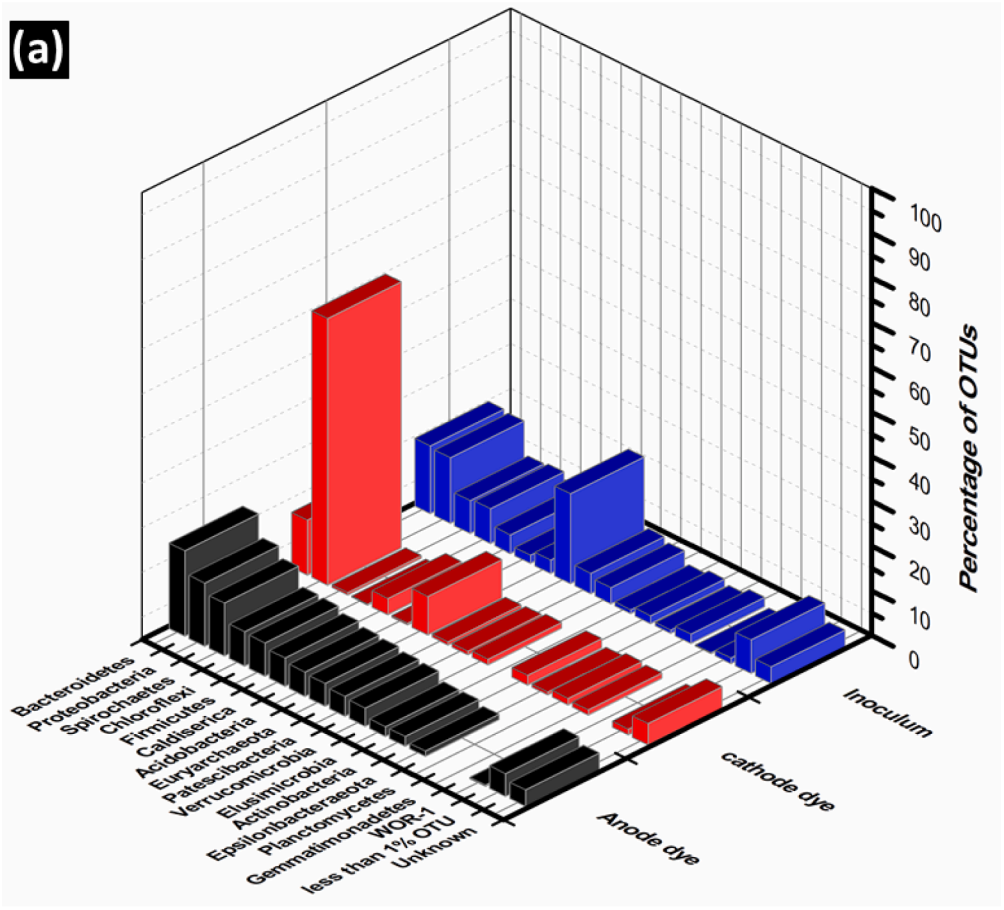

Fig. 6. The microbiological analysis **(a)** based on phylum for anodic, cathodic region and inoculum based on the class level, **(b)** anodic region, **(c)** cathodic region, **(d)** inoculum and **(e)** phylogenetic tree showing the involvement of different species in the dye removal.

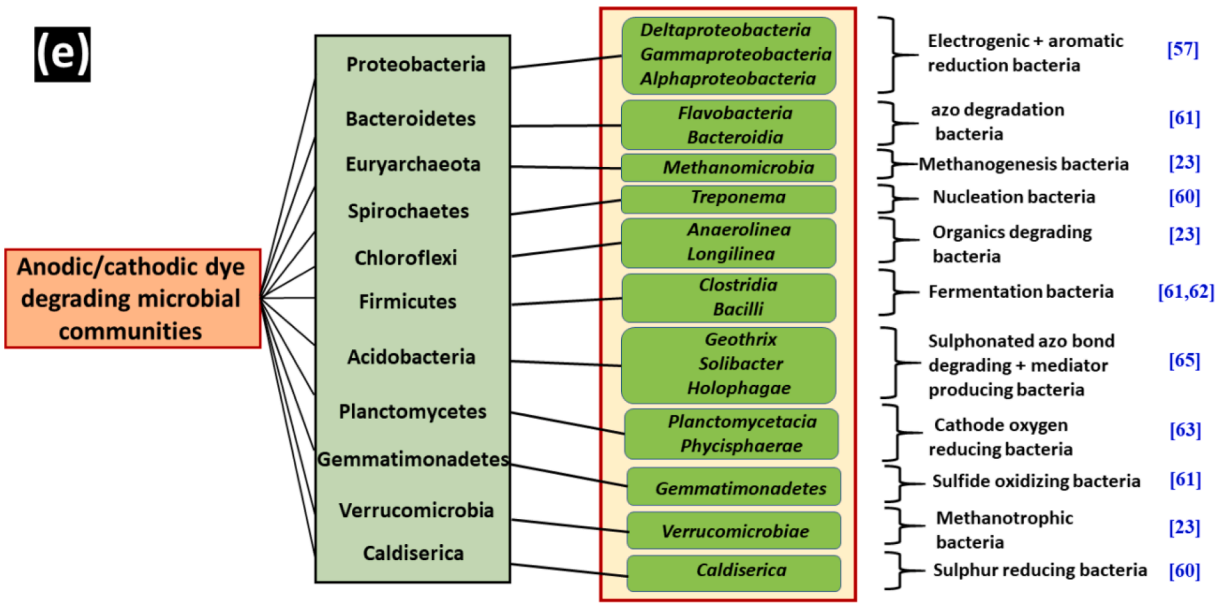

Fig. 6. (*continued*).

to a significant level. Accordingly, present study successfully suggests that cathodic dye effluents were not phyto-toxic, but are relatively safe for the discharge.

3.6. Microbial community analysis

The microbial community analysis of anodic and cathodic samples in comparison to inoculum was characterized by 16S rRNA sequencing. The inoculum for the CW-MFC was found to be more diverse with the operational taxonomic units (OTUs) of 9403 in comparison to anodic and cathodic samples with OTUs of 6568 and 7304, respectively. The Shannon and Chao indices of the inoculum were 5.84 and 1136, respectively. At the same time, anodic and cathodic samples exhibited the Shannon and Chao indices of 5.71 and 683, 5.73 and 588, respectively, suggesting that cathodic and anodic samples exhibited low species diversity and richness compared to inoculum and the results indicate that anodic and cathodic samples were enriched with the selective microbial communities [23]. The most abundant microbial community in anodic samples consisted of phylum *Bacteroidetes* (19.09%) followed by *Proteobacteria* (14.14%), *Spirochaetes* (11.80%), *Chlorofelxi* (7.72%), *Firmicutes* (7.43%), *Caldiserica* (6.26%), *Acidobacteria* (5.39%), *Euryarchaeota* (5.10%), *Patescibacteria* (4.37%), *Verrucomicrobia* (4.08%), *Elusimicrobia* (2.18%), *Actinobacteria* (2.18%), *Epsilonbacteraeota* (1.16%) with the other phyla of lesser than 1%, whereas cathodic community was found to be populated with phylum *Proteobacteria* (59.50%) succeeded by *Bacteroidetes* (12.23%), *Acidobacteria* (8.59%), *Firmicutes* (3.63%), *Actinobacteria* (2.14%), *Verrucomicrobia* (1.32%), *Gemmatimonadetes* (1.157%) and *Planctomycetes* (1.488%) as shown in Fig. 6a. It can be observed from Fig. 6a that some of the microbial communities from inoculum disappeared/shifted in anodic and cathodic samples, which indicates that some of the microbial communities were intolerant to dye wastewater. The abundance of *Proteobacteria*, *Bacteriodetes* as well as *Firmicutes* in anodic samples rather than cathodic samples were also confirmed in the conventional anaerobic digestors as well as in the bioelectrochemical systems [53,54]. In other studies [55], the abundance of *Proteobacteria*, *Bacteroidetes*, *Actinobacteria*, *Planctomycetes*, *Firmicutes* within a bio-cathode of MFC were also recorded, whereas Yang et al., [56] observed a higher abundance of *Euryarchaeota* while treating industrial dye wastewater in a pilot-scale anaerobic reactor. These are also found in the anodic sample of the present study.

Additionally, *Proteobacteria* of the anodic samples were abundant with the class *Deltaproteobacteria* (8.45%), followed by *Gammaproteobacteria* (4.22%), and *Alphaproteobacteria* (1.45%) as shown in Fig. 6b, wherein, *Deltaproteobacteria* were mostly dominant in the anodic samples of CW-MFC. In class *Deltaproteobacteria*, the presence of an *exo*-electrogenic species *Geobacter* (1.16%) was observed, which are obligate anaerobic bacteria (*i.e.,* prefers strictly anaerobic condition). These species are responsible for the extracellular electrons transfer during the organic degradation to promote the electricity generation in bio-electrochemical systems [57]. Additionally, the presence of genus *Desulfovibrio* (2.04%) and *Desulfobulbus* (0.58%) from *Deltaproteobacteria* promoted the electricity generation as it is capable of bidirectional extracellular electron transfer [58].

Contrarily to cathodic samples, the presence of microbes from the phylum *Proteobacteria* followed the sequence of *Gammaproteobacteria* (36.03%) > *Alphaproteobacteria* (22.14%) > *Deltaproteobacteria* (1.32%) as observed in Fig. 6c. The abundance of *Gamma* and *Alpha Proteobacteria* in the cathodic samples when compared to anodic samples indicated the tolerance of these microbes towards MO and the major involvement of *Alpha*, *Beta*, and *Gamma Proteobacteria* microbes were also reported [59] for the degradation of azo dyes. Whereas, other dye degrading microbes include the *Desulfobacterium* from class *Deltaproteobacteria* [60], *Flavobacterium* from class *Bacteriodetes*, *Aminobacter* from class *Alphaproteobacteria*, and *Sphingomonas* belonging to the class *Alphaproteobacteria* [61], were mainly related to aromatic degradation and azo dye reduction. In addition, the OTU abundance of genus *Sphingomonas* was increased from 0.29% to 1.15% in anodic to cathodic samples due to their involvement in aromatic ring degradation of MO. The presence of *Comamonas* species (0.33%) from phylum *Proteobacteria* in the cathodic samples was found to be responsible for degrading aniline aerobically [62].

The abundance of species *Clostridium* from phylum *Firmicutes* in the anodic sample was 7.43%, whereas in the cathodic samples, it was 3.63%. The microbes from the phylum *Firmicutes* mainly played the role in the conversion of complex carbon to simpler molecules and further in the electron transfer process [62]. Likewise, phylum *Choloflexi* was abundant in anodic samples, which was responsible for converting the carbohydrates into electricity [23]. Additionally, the presence of phylum *Planctomycetes* in the cathodic region might have played the role in oxygen reduction, similarfindings were reported in the literature [63].

The inoculum consisted of 2.96% of phylum *Acidobacteria,* but since it is exposed to dye wastewater in the anodic chamber, it was increased to 5.39% and further in the cathodic chamber, it was 8.95% as shown in Fig. 6d. The most abundant genus in the cathodic region belong to *Acidobacteria i.e. Solibacter* (3.63%) species as well as the other species of *Acidithiobacillus*, *Thiomonas*, and *Acidobacteria* genera, which were found to be responsible for the assimilation of sulphur [64]. Moreover, some species of genus *Xanthomonas*, *Acidithiobacillus* and *Thiomonas* were capable of degrading sulfonated azo bonds that can functionalize as azo dye reductase. Additionally, other species like *Desulfobulbus*, *Acidithiobacillus*, and *Thiobacillus* were also capable of degrading aniline via benzoate degradation pathway [65]. Moreover, the detection of species in the cathode related to *Geothrix* genus (1.32%) in *Acidobacteria* phylum can be accounted for producing an unidentified mediator [62,65,66]. However, for a better understanding, a phylogenetic tree was prepared for anodic and cathodic microbial communities showing their involvement in a different process (Fig. 6e).

From the forgoing arguments, it can be deduced that anodic biofilm was rich in electrogenic microbes (EABs-*Proteobacteria*), which are responsible for high organics removal and electricity generation. At the same time, cathode microbial diversity has a high abundance of aromatic compounds reducing bacteria (*Gamma* and *Alpha Proteobacteria*), which can be accounted for the total mineralization of aromatic amines. Moreover, a high abundance of azo dye degrading bacteria (*Bacteriodetes*) and organic degrading bacteria (*Choloroflexi*) justify higher azo bond cleavage and organics removal in the anode, which was contrarily in the cathode with *Choloroflexi* $< 1\%$ owing to lesser organic content remaining in the cathode. Additionally, as the bottom of the anode chamber was fed with a high concentration of organics with fresh incoming wastewater, thus it has the majority of fermentative bacteria (*Firmicutes*), which helps in the oxidation of the substrate. In consequence of the anaerobic conditions in the anode, *Planctomycetes* were totally absent, but were identified in the cathode due to its functioning as the cathode oxygen reducing bacteria. Also, methanogenesis bacteria (*Verrucomicrobia* and *Methanomicrobia*) were evident in the anode due to low DO profile contrary to the cathode.

4. Conclusions

An innovative design of the earthen membrane-based two chambers CW-MFC with the sequential anaerobic and aerobic regimes proved its potential for an efficient removal of MO azo dye containing wastewater with a simultaneous electricity generation of 148.29 mW/m^3. This two-chambered earthen membrane-based CW-MFC was found to be beneficial compared to a single-chambered CW-MFC, which achieved 94.04 $\pm$ 2.87% COD removal and 94.22 $\pm$ 1.33% azo dye removal. The results further indicated high COD and azo dye removal in anodic and cathodic regions, which played an important role for the complete mineralization of MO aromatic intermediates to lesser harmful and non-toxic products. Toxicity data corroborated with the reduction of phytotoxicity levels in anodic and cathodic effluents by displaying the root growth of 18.62 $\pm$ 10.51% and 54.75 $\pm$ 14.98%, respectively in comparison to tap water control, which was performed with three different seeds. A comparison of Shannon and Chao indices between anodic, cathodic, and inoculum OTUs revealed the selective enrichment of dye degrading, aromatic reducing, cathode oxygen reducing, and electrochemically active microbial communities in anodic and cathodic regions. In view of the higher performance by the earthen membrane-based two chambered unplanted CW-MFC, it can be further explored in the context of real textile dye wastewater, addition of vegetation, packaging substrate, pilot scale implementation and workable energy harvesting aspects. Besides, clogging assessment can also be evaluated, which is one of the common challenges in CWs. Moreover, the impact of numerous other factors such as (i) thickness of the earthen pot membrane, (ii) electrode distancing and (iii) siphoning effect, on the azo dye removal can be evaluated.

Declaration of Competing Interest

The authors declare that they have no known competing financial interests or personal relationships that could have appeared to influence the work reported in this paper.

Acknowledgments

Yamini Mittal acknowledges the GATE-SRF fellowship provided by the Council of Scientific and Industrial Research (CSIR), India. She is also thankful to AcSIR, New Delhi, for helping her to carry out Ph.D. work. Asheesh Kumar Yadav is grateful to CSIR-IMMT for providing all the facilities and infrastructure (MLP-059 and MLP-057) for the execution of the work.

Also, this work has been submitted for patent application in India on 8th February 2021 with the file number- 202111005592.

Appendix A. Supplementary data

Supplementary data to this article can be found online at https://doi.org/10.1016/j.cej.2021.131856.

References

[1] F. Kong, H.-Y. Ren, S.G. Pavlostathis, A. Wang, J. Nan, N.-Q. Ren, Enhanced azo dye decolorization and microbial community analysis in a stacked bioelectrochemical system, Chem. Eng. J. 354 (2018) 351–362.
[2] M. Fatima, R. Farooq, R.W. Lindström, M. Saeed, A review on biocatalytic decomposition of azo dyes and electrons recovery, J. Mol. Liq. 246 (2017) 275–281.
[3] S. Xie, P. Huang, J.J. Kruzic, X. Zeng, H. Qian, A highly efficient degradation mechanism of methyl orange using Fe-based metallic glass powders, Sci. Rep. 6 (2016) 1–10.
[4] Y. Mu, K. Rabaey, R.A. Rozendal, Z. Yuan, J. Keller, Decolorization of azo dyes in bioelectrochemical systems, Environ. Sci. Technol. 43 (13) (2009) 5137–5143.
[5] L. Ayed, E. Khelifi, H.B. Jannet, H. Miladi, A. Cheref, S. Achour, A. Bakhrouf, Response surface methodology for decolorization of azo dye Methyl Orange by bacterial consortium: produced enzymes and metabolites characterization, Chem. Eng. J. 165 (2010) 200–208.
[6] B.E.L. Baêta, D.R.S. Lima, S.Q. Silva, S.F. Aquino, Evaluation of soluble microbial products and aromatic amines accumulation during a combined anaerobic/aerobic treatment of a model azo dye, Chem. Eng. J. 259 (2015) 936–944.
[7] F.P. van der Zee, S. Villaverde, Combined anaerobic–aerobic treatment of azo dyes—a short review of bioreactor studies, Water Res. 39 (8) (2005) 1425–1440.
[8] T.A. Nguyen, R.-S. Juang, Treatment of waters and wastewaters containing sulfur dyes: a review, Chem. Eng. J. 219 (2013) 109–117.
[9] S. Gupta, Y. Mittal, P. Tamta, P. Srivastava, A.K. Yadav, Textile wastewater treatment using microbial fuel cell and coupled technology: a green approach for detoxification and bioelectricity generation, in: Integrated Microbial Fuel Cells for Wastewater Treatment, Elsevier, 2020: pp. 73–92.
[10] P. Srivastava, R. Abbassi, V. Garaniya, T. Lewis, Y. Zhao, T. Aminabhavi, Interrelation between sulphur and conductive materials and its impact on ammonium and organic pollutants removal in electroactive wetlands, J. Hazard. Mater. 419 (2021), 126417.
[11] J. Vymazal, Constructed wetlands for treatment of industrial wastewaters: a review, Ecol. Eng. 73 (2014) 724–751.
[12] A.K. Yadav, N. Kumar, T. Sreekrishnan, S. Satya, N.R. Bishnoi, Removal of chromium and nickel from aqueous solution in constructed wetland: mass balance, adsorption–desorption and FTIR study, Chem. Eng. J. 160 (2010) 122–128.
[13] P. Srivastava, A.K. Yadav, V. Garaniya, R. Abbassi, Constructed wetland coupled microbial fuel cell technology: development and potential applications, in: Microbial Electrochemical Technology, Elsevier, 2019: pp. 1021–1036.
[14] A.K. Yadav, P. Dash, A. Mohanty, R. Abbassi, B.K. Mishra, Performance assessment of innovative constructed wetland-microbial fuel cell for electricity production and dye removal, Ecol. Eng. 47 (2012) 126–131, https://doi.org/10.1016/j.ecoleng.2012.06.029.
[15] A.K. Yadav, P. Srivastava, N. Kumar, R. Abbassi, B.K. Mishra, Constructed wetland-microbial fuel cell: an emerging integrated technology for potential industrial wastewater treatment and Bio-electricity generation, Constructed Wetlands for Industrial Wastewater Treatment. (2018) 493–510.
[16] P. Srivastava, R. Abbassi, A.K. Yadav, V. Garaniya, M.A.F. Jahromi, A review on the contribution of an electron in electroactive wetlands: electricity generation and enhanced wastewater treatment, Chemosphere 126926 (2020).
[17] A. Yadav, Design and development of novel constructed wetland cum microbial fuel cell for electricity production and wastewater treatment, in: 2010: pp. 4–10.
[18] S. Gupta, P. Srivastava, A.K. Yadav, Simultaneous removal of organic matters and nutrients from high-strength wastewater in constructed wetlands followed by entrapped algal systems, Environ. Sci. Pollut. Res. 27 (1) (2020) 1112–1117.

[19] R. Liu, Y. Zhao, L. Doherty, Y. Hu, X. Hao, A review of incorporation of constructed wetland with other treatment processes, Chem. Eng. J. 279 (2015) 220–230.
[20] Z. Fang, H.-L. Song, N. Cang, X.-N. Li, Performance of microbial fuel cell coupled constructed wetland system for decolorization of azo dye and bioelectricity generation, Bioresour. Technol. 144 (2013) 165–171.
[21] Z. Fang, H.-liang. Song, N. Cang, X.-ning. Li, Electricity production from Azo dye wastewater using a microbial fuel cell coupled constructed wetland operating under different operating conditions, Biosens. Bioelectron. 68 (2015) 135–141.
[22] Z. Fang, H. Song, R. Yu, X. Li, A microbial fuel cell-coupled constructed wetland promotes degradation of azo dye decolorization products, Ecol. Eng. 94 (2016) 455–463.
[23] R. Rathour, D. Patel, S. Shaikh, C. Desai, Eco-electrogenic treatment of dyestuff wastewater using constructed wetland-microbial fuel cell system with an evaluation of electrode-enriched microbial community structures, Bioresour. Technol. 285 (2019), 121349.
[24] Y.-L. Oon, S.-A. Ong, L.-N. Ho, Y.-S. Wong, F.A. Dahalan, Y.-S. Oon, T.-P. Teoh, H. K. Lehl, W.-E. Thung, Constructed wetland–microbial fuel cell for azo dyes degradation and energy recovery: Influence of molecular structure, kinetics, mechanisms and degradation pathways, Sci. Total Environ. 720 (2020), 137370.
[25] R. Regmi, R. Nitisoravut, S. Charoenroongtavee, W. Yimkhaophong, O. Phanthurat, Earthen pot–plant microbial fuel cell powered by Vetiver for bioelectricity production and wastewater treatment, CLEAN–Soil, Air Water. 46 (2018) 1700193.
[26] P.S. Jana, M. Behera, M.M. Ghangrekar, Performance comparison of up-flow microbial fuel cells fabricated using proton exchange membrane and earthen cylinder, Int. J. Hydrogen Energy 35 (11) (2010) 5681–5686.
[27] Y. Yang, Y. Zhao, C. Tang, Y. Mao, C. Shen, Significance of water level in affecting cathode potential in electro-wetland, Bioresour. Technol. 285 (2019), 121345.
[28] American Public Health Association, APHA (2005) Standard methods for the examination of water and wastewater, APHA Washington DC, USA. (2005).
[29] P. Tamta, N. Rani, A.K. Yadav, Enhanced wastewater treatment and electricity generation using stacked constructed wetland–microbial fuel cells, Environ. Chem. Lett. 18 (3) (2020) 871–879.
[30] P. Srivastava, S. Dwivedi, N. Kumar, R. Abbassi, V. Garaniya, A.K. Yadav, Performance assessment of aeration and radial oxygen loss assisted cathode based integrated constructed wetland-microbial fuel cell systems, Bioresour. Technol. 244 (2017) 1178–1182.
[31] Y. Pan, Y. Wang, A. Zhou, A. Wang, Z. Wu, L. Lv, X. Li, K. Zhang, T. Zhu, Removal of azo dye in an up-flow membrane-less bioelectrochemical system integrated with bio-contact oxidation reactor, Chem. Eng. J. 326 (2017) 454–461.
[32] C. Tang, Y. Zhao, C. Kang, Y. Yang, D. Morgan, L. Xu, Towards concurrent pollutants removal and high energy harvesting in a pilot-scale CW-MFC: Insight into the cathode conditions and electrodes connection, Chem. Eng. J. 373 (2019) 150–160.
[33] J.M. Morris, S. Jin, B. Crimi, A. Pruden, Microbial fuel cell in enhancing anaerobic biodegradation of diesel, Chem. Eng. J. 146 (2) (2009) 161–167.
[34] Q. Wen, F. Kong, H. Zheng, J. Yin, D. Cao, Y. Ren, G. Wang, Simultaneous processes of electricity generation and ceftriaxone sodium degradation in an air-cathode single chamber microbial fuel cell, J. Power Sour. 196 (5) (2011) 2567–2572.
[35] J. Fan, Y. Guo, J. Wang, M. Fan, Rapid decolorization of azo dye methyl orange in aqueous solution by nanoscale zerovalent iron particles, J. Hazard. Mater. 166 (2-3) (2009) 904–910.
[36] V. Murali, S.-A. Ong, L.-N. Ho, Y.-S. Wong, Evaluation of integrated anaerobic–aerobic biofilm reactor for degradation of azo dye methyl orange, Bioresour. Technol. 143 (2013) 104–111.
[37] J. Sun, Y.-you. Hu, Z. Bi, Y.-qing. Cao, Simultaneous decolorization of azo dye and bioelectricity generation using a microfiltration membrane air-cathode single-chamber microbial fuel cell, Bioresour. Technol. 100 (13) (2009) 3185–3192.
[38] C.-C. Hsueh, B.-Y. Chen, Comparative study on reaction selectivity of azo dye decolorization by Pseudomonas luteola, J. Hazard. Mater. 141 (3) (2007) 842–849.
[39] G. Chen, K.Y. Cheng, M.P. Ginige, A.H. Kaksonen, Aerobic degradation of sulfanilic acid using activated sludge, Water Res. 46 (1) (2012) 145–151.
[40] P.-J. Cai, X. Xiao, Y.-R. He, W.-W. Li, J. Chu, C. Wu, M.-X. He, Z. Zhang, G.-P. Sheng, M.-W. Lam, F. Xu, H.-Q. Yu, Anaerobic biodecolorization mechanism of methyl orange by Shewanella oneidensis MR-1, Appl. Microbiol. Biotechnol. 93 (4) (2012) 1769–1776.
[41] G.K. Parshetti, A.A. Telke, D.C. Kalyani, S.P. Govindwar, Decolorization and detoxification of sulfonated azo dye methyl orange by Kocuria rosea MTCC 1532, J. Hazard. Mater. 176 (1-3) (2010) 503–509.
[42] Y.-P. Chen, S.-Y. Liu, H.-Q. Yu, H. Yin, Q.-R. Li, Radiation-induced degradation of methyl orange in aqueous solutions, Chemosphere 72 (4) (2008) 532–536.
[43] H. Zou, Y. Wang, Functional collaboration of biofilm-cathode electrode and microbial fuel cell for biodegradation of methyl orange and simultaneous bioelectricity generation, Environ. Sci. Pollut. Res. 26 (22) (2019) 23061–23069.
[44] A.F. Al-Rubaye, M.J. Kadhim, I.H. Hameed, Phytochemical profiles of methanolic seeds extract of Cuminum cyminum using GC-MS technique, Int. J. Current Pharm. Review Resear. 8 (2017) 114–124.
[45] N. Supaka, K. Juntongjin, S. Damronglerd, M. Delia, P. Strehaiano, Microbial decolorization of reactive azo dyes in a sequential anaerobic–aerobic system, Chem. Eng. J. 99 (2) (2004) 169–176.
[46] Z. Fang, S. Cheng, H. Wang, X. Cao, X. Li, Feasibility study of simultaneous azo dye decolorization and bioelectricity generation by microbial fuel cell-coupled constructed wetland: substrate effects, RSC Adv. 7 (27) (2017) 16542–16552.
[47] Y.-L. Oon, S.-A. Ong, L.-N. Ho, Y.-S. Wong, F.A. Dahalan, Y.-S. Oon, H.K. Lehl, W.-E. Thung, N. Nordin, Up-flow constructed wetland-microbial fuel cell for azo dye, saline, nitrate remediation and bioelectricity generation: from waste to energy approach, Bioresour. Technol. 266 (2018) 97–108.
[48] D. Patel, S.L. Bapodra, D. Madamwar, C. Desai, Electroactive bacterial community augmentation enhances the performance of a pilot scale constructed wetland microbial fuel cell for treatment of textile dye wastewater, Bioresour. Technol. 332 (2021), 125088.
[49] P. Srivastava, R. Abbassi, V. Garaniya, T. Lewis, A.K. Yadav, Performance of pilot-scale horizontal subsurface flow constructed wetland coupled with a microbial fuel cell for treating wastewater, J. Water Process Eng. 33 (2020), 100994.
[50] H. Rismani-Yazdi, S.M. Carver, A.D. Christy, O.H. Tuovinen, Cathodic limitations in microbial fuel cells: an overview, J. Power Sour. 180 (2) (2008) 683–694.
[51] S.-M. Tan, S.-A. Ong, L.-N. Ho, Y.-S. Wong, C.Z.A. Abidin, W.-E. Thung, T.-P. Teoh, Biotreatment of sulfonated dyestuffs with energy recovery in microbial fuel cell: Influencing parameters, kinetics, degradation pathways, mechanisms, and phytotoxicity assessment, J. Environ. Chem. Eng. 9 (2021), 105525.
[52] R. Abbassi, A.K. Yadav, N. Kumar, S. Huang, P.R. Jaffe, Modeling and optimization of dye removal using "green" clay supported iron nano-particles, Ecol. Eng. 61 (2013) 366–370.
[53] P. Srivastava, R. Abbassi, A. Kumar Yadav, V. Garaniya, N. Kumar, S.J. Khan, T. Lewis, Enhanced chromium (VI) treatment in electroactive constructed wetlands: influence of conductive material, J. Hazard. Mater. 387 (2020) 121722, https://doi.org/10.1016/j.jhazmat.2019.121722.
[54] P. Srivastava, A.K. Yadav, V. Garaniya, T. Lewis, R. Abbassi, S.J. Khan, Electrode dependent anaerobic ammonium oxidation in microbial fuel cell integrated hybrid constructed wetlands: A new process, Sci. Total Environ. 698 (2020) 134248, https://doi.org/10.1016/j.scitotenv.2019.134248.
[55] G.-W. Chen, S.-J. Choi, J.-H. Cha, T.-H. Lee, C.-W. Kim, Microbial community dynamics and electron transfer of a biocathode in microbial fuel cells, Korean J. Chem. Eng. 27 (5) (2010) 1513–1520.
[56] B. Yang, H. Xu, S. Yang, S. Bi, F. Li, C. Shen, C. Ma, Q. Tian, J. Liu, X. Song, W. Sand, Y. Liu, Treatment of industrial dyeing wastewater with a pilot-scale strengthened circulation anaerobic reactor, Bioresour. Technol. 264 (2018) 154–162.
[57] F. Rezaei, T.L. Richard, B.E. Logan, Enzymatic hydrolysis of cellulose coupled with electricity generation in a microbial fuel cell, Biotechnol. Bioeng. 101 (6) (2008) 1163–1169.
[58] M.-H. Cui, D. Cui, L. Gao, H.-Y. Cheng, A.-J. Wang, Analysis of electrode microbial communities in an up-flow bioelectrochemical system treating azo dye wastewater, Electrochim. Acta 220 (2016) 252–257.
[59] Y.M. Kolekar, H.N. Nemade, V.L. Markad, S.S. Adav, M.S. Patole, K.M. Kodam, Decolorization and biodegradation of azo dye, reactive blue 59 by aerobic granules, Bioresour. Technol. 104 (2012) 818–822.
[60] A. Kuppardt, S. Kleinsteuber, C. Vogt, T. Lüders, H. Harms, A. Chatzinotas, Phylogenetic and functional diversity within toluene-degrading, sulphate-reducing consortia enriched from a contaminated aquifer, Microb. Ecol. 68 (2) (2014) 222–234.
[61] T. Li, Z. Fang, R. Yu, X. Cao, H. Song, X. Li, The performance of the microbial fuel cell-coupled constructed wetland system and the influence of the anode bacterial community, Environ. Technol. 37 (13) (2016) 1683–1692.
[62] Y. Wang, Y. Pan, T. Zhu, A. Wang, Y. Lu, L. Lv, K. Zhang, Z. Li, Enhanced performance and microbial community analysis of bioelectrochemical system integrated with bio-contact oxidation reactor for treatment of wastewater containing azo dye, Sci. Total Environ. 634 (2018) 616–627.
[63] H. Zhang, Q. Wen, Z. An, Z. Chen, J. Nan, Analysis of long-term performance and microbial community structure in bio-cathode microbial desalination cells, Environ. Sci. Pollut. Res. 23 (6) (2016) 5931–5940.
[64] N. Devpura, K. Jain, A. Patel, C.G. Joshi, D. Madamwar, Metabolic potential and taxonomic assessment of bacterial community of an environment to chronic industrial discharge, Int. Biodeterior. Biodegrad. 123 (2017) 216–227.
[65] T. Ito, Y. Adachi, Y. Yamanashi, Y. Shimada, Long–term natural remediation process in textile dye–polluted river sediment driven by bacterial community changes, Water Res. 100 (2016) 458–465.
[66] P. Srivastava, R. Abbassi, A. Yadav, V. Garaniya, M. Asadnia, T. Lewis, S.J. Khan, Influence of applied potential on treatment performance and clogging behaviour of hybrid constructed wetland-microbial electrochemical technologies, Chemosphere 284 (2021) 131296, https://doi.org/10.1016/j.chemosphere.2021.131296.